Journal of Alloys and Compounds 512 (2012) 5–11

Contents lists available at ScienceDirect

Journal of Alloys and Compounds

journal homepage: www.elsevier.com/locate/jallcom

Preparation of Dy^{3+}-activated strontium orthosilicate (Sr_2SiO_4:Dy^{3+}) phosphors and its photoluminescent properties

Le Zhang [a], Zhou Lu [a], Hao Yang [a], Pengde Han [a], Naicen Xu [b,a], Qitu Zhang [a,*]

[a] College of Materials Science and Engineering, Nanjing University of Technology, Nanjing 210009, China
[b] Nanjing Institute of Geology and Mineral Resources, Nanjing 210016, China

ARTICLE INFO

Article history:
Received 9 March 2011
Received in revised form 26 July 2011
Accepted 28 July 2011
Available online 3 August 2011

Keywords:
Sr_2SiO_4:Dy^{3+}
Solid state reaction
White light emitting diodes
Luminescence

ABSTRACT

Dy^{3+}-activated β/α′-Sr_2SiO_4 phosphors were successfully prepared by solid-state reaction method with ammonium chloride (NH_4Cl) as the flux. The influences of calcination temperatures, amounts of NH_4Cl and the concentrations of Dy^{3+} on phase composition, morphology and the photoluminescent properties of as-prepared powders were investigated in detail. The β and α′ phases of Sr_2SiO_4 were obtained with 1 wt% and 2–5 wt% NH_4Cl, respectively, as the sintered condition was at 1000 °C for 4 h. With increasing the amount of NH_4Cl, the morphology of phosphors changed from needlelike to regular polyhedron shape and the colors of the Sr_2SiO_4:Dy^{3+} phosphors changed from blue-green to white. The luminescence intensity of $^4F_{9/2} \rightarrow {}^6H_{15/2}$ transition was slightly higher than that of $^4F_{9/2} \rightarrow {}^6H_{13/2}$ ($\Delta L = 2$, $\Delta J = 2$) transition owing to the low-symmetry around Dy^{3+} ions. The optimum concentration of Dy^{3+} was 2.0 mol% and the concentration quenching were caused by the d–d interaction and a cross relaxation. The yellow-to-blue intensity ratio (Y/B) of Dy^{3+} emission did not to change with varying the Dy^{3+} concentration using Li^+ ions for charge compensation. These indicate that this phosphor can be used as a potential candidate for the phosphor-converted white LEDs with a UV chip.

1. Introduction

White light generation through InGaN-based light emitting diodes (LED) has numerous advantages over the existing incandescent and fluorescent lamps in power efficiency, small size, light weight, long lifetime and flat packaging [1,2]. There are several technologies that combined blue/ultraviolet (UV) LED and phosphors to generate white light [3,4]. The first white LED consists of blue LED chips and yellow YAG:Ce^{3+} phosphor, which exhibits high luminescent efficiency and chemical stability but a deviated natural white light due to halo effect of blue/yellow color separation and lower color rendering index (Ra) of ~80 caused by the lack of red emission [5–8]. The combination of UV LED chips and the red/green/yellow/blue light emitted from the phosphors provides superior color uniformity with a high color rendering index and excellent quality of light [9]. But the luminous efficiency of the latter white LED has severely depended on the light reabsorption and the matching ratios among different color phosphors [4,9]. Therefore, it is necessary to find new phosphors that can be effectively excited in the (N-) UV range and can emit white light, which are known as single matrix white phosphors (SMWP).

At present, the most of SMWP candidates focus on aluminate, borate, and especially silicate matrix such as $Ba_3MgSi_2O_8$:Eu^{2+}, Mn^{2+} [10], $Sr_3MgSi_2O_8$:Eu^{2+} [11], $Sr_3MgSi_2O_8$:Eu^{2+}, Mn^{2+} [12], $BaMgAl_{10}O_{17}$:Eu^{2+}, Mn^{2+} (BAM) [13], and $Sr_3B_2O_6$:Eu^{2+}, Ce^{3+} [14,15]. The silicate matrix has the merits of the stability under high power UV radiation and the durability in the packaging resin. Alkaline earth orthosilicates M_2SiO_4 (M = Sr, Ca, Ba) doped with Eu^{2+} have been well documented and their emission intensities and colors vary with the crystal field and the covalence around the activator ions, especially, the crystal phase α′ or β of the host [16–18]. The preparation of single phase alkaline earth orthosilicate with higher luminescent efficiency for doped rare earth ions is thus our main task.

Meanwhile, Dy^{3+} ions with two dominant bands in their emission spectra are known as natural white light emitting ions. The blue band (485 nm) corresponds to the $^4F_{9/2} \rightarrow {}^6H_{15/2}$ transition and the yellow band (570 nm) corresponds to the hypersensitive $^4F_{9/2} \rightarrow {}^6H_{13/2}$ transition ($\Delta L = 2$, $\Delta J = 2$), and the intensity of the yellow band is dependent on the lattice site of the host. Thus, seeking a phosphor of Dy^{3+} ions doped compounds, in which Dy^{3+} would emit white light with a suitable intensity ratio of yellow to blue and acceptable luminescence efficiency, never ceased [19]. In this paper, we strives to prepare single phase Dy^{3+}-activated strontium orthosilicate (Sr_2SiO_4:Dy^{3+}) phosphor and investigate its luminescent properties to discuss the possibility of Sr_2SiO_4:Dy^{3+} powders as the white LED materials. Pure α′-Sr_2SiO_4:Dy^{3+} phosphors with

* Corresponding author. Tel.: +86 25 83587246; fax: +86 25 83587246.
E-mail addresses: njutzl@163.com (L. Zhang), zhqt@njut.edu.cn (Q. Zhang).

0925-8388/$ – see front matter © 2011 Published by Elsevier B.V.
doi:10.1016/j.jallcom.2011.07.089

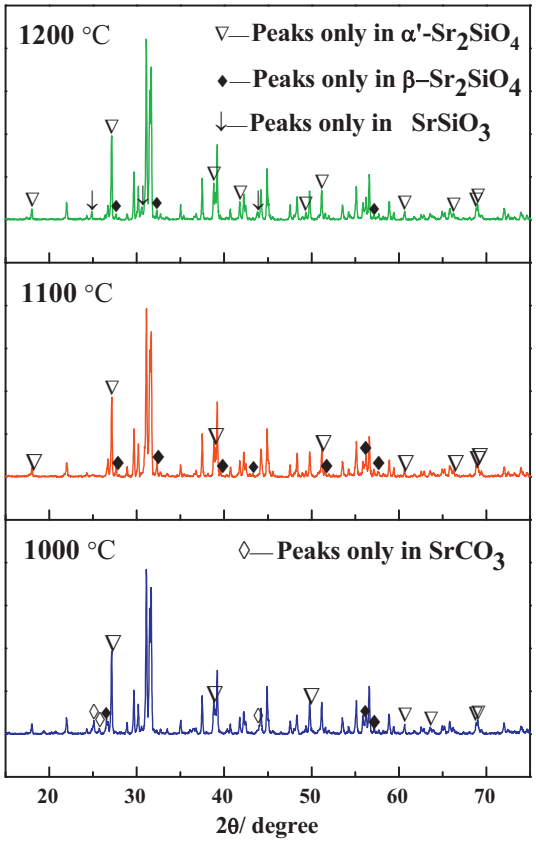

Fig. 1. XRD patterns of $(Sr_{0.99}Dy_{0.01})_2SiO_4$ phosphors treated at various temperatures without flux.

2–5 wt% NH_4Cl as flux could emit bright white light and it may be used as the potential two-band SMWP.

2. Materials and experimental details

All powder samples were synthesized through the solid-state reaction technique. High pure $SrCO_3$ (AR), SiO_2 (AR), Dy_2O_3 (>99.99%), Li_2CO_3 (AR), NH_4Cl (AR) were used as starting materials. Stoichiometrical amount of starting materials using Li_2CO_3 for charge compensation and various amounts of NH_4Cl as the flux were mixed thoroughly in alcohol by ball milling in agate mortar and then dried. The synthesis was performed at 900–1300 °C for 4 h in the electric furnace. Serious of $(Sr_{1-x})_2SiO_4$:Dy_{2x} powders were prepared. For comparison, commercial phosphors, YAG:Ce^{3+} and Sr_2SiO_4:Eu^{2+}, are purchased from Luming Luminous Technology Co., Ltd., Dalian, China.

Differential scanning calorimetry (DSC) and thermal gravimetric analyses (TG) of the precursor were made on the Simultaneous Thermal Analysis (STA-449 C, Netzsch, Germany) with a heating rate 10 °C/min and upper temperature limit of 1300 °C. The crystalline phases of synthesized powders were determined by X-ray diffraction (XRD, D/Max2500, Rigaku, Japan) using Cu Kα radiation (λ = 1.5406 Å) in the range of 5–80° with a step size of 0.02°. Crystal structure refinement employed the Rietveld method as implanted in the General Structure Analysis System (GSAS) software suite [20,21]. Powder particle morphology analysis was carried out by scanning electron microscopy (SEM, JSM-5900, NEC, Japan). The photoluminescence spectra of the phosphors were measured using a fluorescent spectrophotometer (FL3-221, HOROBA, Jobin Yvon, France) at room temperature.

3. Results and discussion

3.1. Preparation of pure and single-phase $(Sr_{0.99}Dy_{0.01})_2SiO_4$ phosphors

3.1.1. Effect of different calcination temperatures without flux

The XRD patterns of the phosphors calcined at desired temperatures are exhibited in Fig. 1. Because the overlap regions between the diffraction peaks of α′-Sr_2SiO_4 (JCPDS #39-1256) and β-Sr_2SiO_4 (JCPDS #38-0271) are too much to index them precisely, especially around the strongest peak around 30–32°. So we indexed the diffraction peaks with significant distinction comparing to the others. The phase composition of the formed powders was major α′-Sr_2SiO_4 and certain number of β-Sr_2SiO_4 with minor undecomposed $SrCO_3$ (JCPDS #05-0418) as heat treated at 1000 °C. As the heat treated temperature was 1100 °C, the formed phases were nearly equal amount of α′-Sr_2SiO_4 and β-Sr_2SiO_4 but $SrCO_3$ disappeared. Furthermore, the $SrSiO_3$ (JCPDS #36-0018) appeared at the heat treated temperature 1200 °C. When heating temperature keep heightening, the composition included two phases at least, α′-Sr_2SiO_4 and β-Sr_2SiO_4 (not shown here). That is, the pure α′-Sr_2SiO_4 or β-Sr_2SiO_4 phosphor could not been obtained only changing heating temperature in our experiments. Fig. 2 shows the SEM morphologies of corresponding powders. The morphologies of the powders did change significantly with changing heating temperatures. The powders prepared at 1000 °C for 4 h consisted of relatively well-dispersed and uniform crystals with a needle-like shape (Fig. 2(a)). However, the morphology of the powders prepared at 1100 °C, 1200 °C or1300 °C for 4 h was irregular, which had a growing primary particle size of 0.5–1 μm. Simultaneously, these particles were seriously sintered to large platelike agglomerates of several micrometers because of high temperature. For practical applications, the phosphor particles with a uniform size and spherical like shape are highly desired, which are beneficial to a highly efficient and uniform luminescence. Neither the needle-like particles nor the large agglomerate particles in Fig. 2(b)–(d) is what we want. Although we do not know the reason of significant changes in morphology precisely, it seems that a lower temperature is more advantageous to obtaining finer particles. To our disappointment, the results obtained using present technique strongly suggest that some changes must be attempted to obtain the pure α′-Sr_2SiO_4 or β-Sr_2SiO_4 phosphors with desired morphology.

3.1.2. Adding different amounts of NH_4Cl flux

Usually, in the most of solid state reaction for synthesizing silicate phosphors, such fluxes as halide (KCl, $CaCl_2$), B_2O_3, and boron compounds are added to improve the sintering process and then decrease the calcination temperature by forming liquid phase and absorbing impurities from grain interior, simultaneously. For NH_4Cl, it was water-soluble and easy to be separated from phosphors. Especially, even at higher concentration, the second phase such as alkaline-earth chloride and other impurities were easily removed only by washing in hot water, which was very important for higher luminescent efficiency. In our previous work, B_2O_3 and halide were successively selected as the flux materials (not shown here). But the single-phase powder was not obtained till we met NH_4Cl. The addition of B_2O_3 and halide ($CaCl_2$) still remained the co-existence of α′ and β phases in Sr_2SiO_4 powders, regardless of the amount more or less. And the by-product such as CaB_2O_4 was unexpected and it was infeasible to remove by washing. In addition, NH_4Cl can greatly enhance the intensity of phosphor than Li_2CO_3, Na_2CO_3 or K_2CO_3 for some phosphors [22–24]. Here, various amounts of NH_4Cl were thus selected to be added into precursors and then sintered at 1000 °C for 4 h. The XRD patterns of corresponding phosphors are presented in Fig. 3. To our excited, the crystalline phase of the sample with 1.0 wt% NH_4Cl was single β phase. And with the amounts of NH_4Cl flux 2.0 wt% and 5.0 wt%, the as-prepared powders only contained single α′ phase. However, an excessive NH_4Cl of 10.0 wt% would promote the formation of chloro-silicate like $Sr_5SiO_7Cl_4$ with a certain amount of $SrSiO_3$ and SiO_2 as byproducts. The results indicate that the phase compositions are strong dependent on the amounts of NH_4Cl. We selected the XRD of the samples with 1.0 wt% and 5.0 wt% NH_4Cl to fit using Rietveld method. The starting models for the refinements of the phases were taken from β-Sr_2SiO_4 and α′-Sr_2SiO_4 with space groups of *P21/n* and *Pnma*, respectively. The profile was fitted

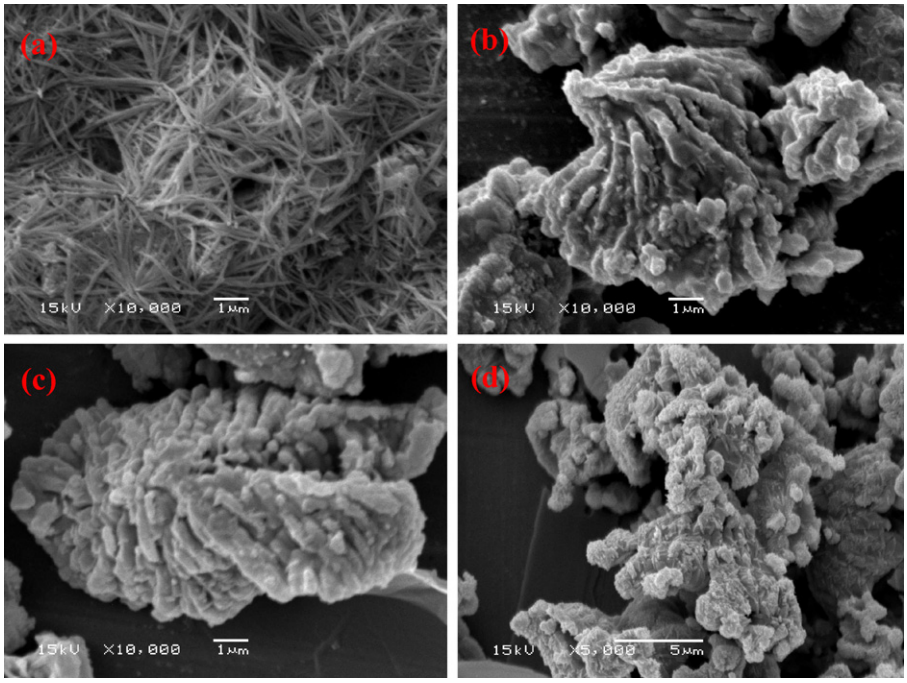

Fig. 2. SEM photographs of the $(Sr_{0.99}Dy_{0.01})_2SiO_4$ phosphors treated at (a) 1000 °C, (b) 1100 °C, (c) 1200 °C and (d) 1300 °C for 4 h, respectively, without flux.

using Pseudo–Voigt profile function. Fig. 4 shows the typical best fit that was observed, calculated, the difference powders diffraction profiles and the expected Bragg reflections for corresponding samples. The refined *R*-values were 12.65/11.54 (R_{wp}%), and 9.38/7.92 (R_p%) and $\chi^2 = 4.339/3.782$ for β/α′ phase, which suggested that the refinements was in good agreement with the space group in all respects. The cell parameters were $a = 5.6603(2)/5.6680(3)$, $b = 7.0796(1)/7.0751(2)$, and $c = 9.7533(1)/9.7357(3)$ for β/α′. All these proved that the single β- or α′-Sr_2SiO_4 is successfully obtained only by changing the amount of flux.

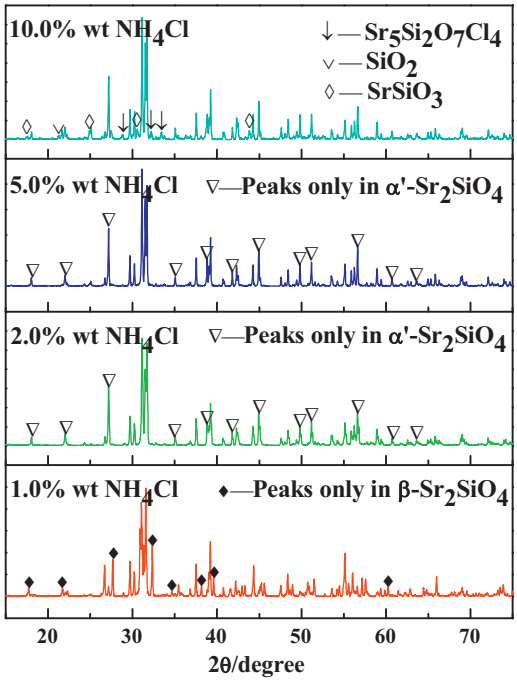

Fig. 3. XRD patterns of $(Sr_{0.99}Dy_{0.01})_2SiO_4$ phosphors treated at 1000 °C for 4 h as s function of the mass fraction of NH_4Cl.

As we know, the structures of β- (monoclinic) and α′-Sr_2SiO_4 (orthorhombic) are same with those of Ca_2SiO_4 and β-K_2SO_4, respectively, and their transition temperature is about 358 K [25]. Only by solid state reaction method, the single and pure β- or α′ phase is difficult to obtain, which is proved by series of reports [17,26–28] and our above results (Fig. 1).

Kim [25] and Sun [29] found the phase transformation from β to α′-Sr_2SiO_4 by increasing the Eu^{2+} concentration (single β phase formed as $x \leq 0.005$ and αĭ phase when $x > 0.01$). Pan [30] had also obtained the α′-$Ba_{0.1}Sr_{1.9}SiO_4$:Eu^{2+} under 1300 for 3 h but Ba-free Sr_2SiO_4:Eu^{2+} had a secondary β phase. Kang [31] obtained the α′ phase using spray pyrolysis method when without flux and the amount of NH_4Cl flux 6 wt%, but 1–5% wt NH_4Cl addition made the phase consist of major β phase and minor α′ phase. Even using the same synthesis method and also using the same flux NH_4Cl, Kim [25] reported that the synthesized Sr_2SiO_4:Eu^{2+} fired at 800 °C for 3 h under 5%H_2 with 1 wt% NH_4Cl was a single α′ phase with little Eu_2O_3. Even adding 2–10 wt% NH_4Cl, the crystalline phase was still α′ phase. While we only added 1.0 wt% and 2.0–5.0 wt% NH_4Cl and then fired the precursor at 1000 °C for 4 h, β and α′-Sr_2SiO_4 were successfully obtained, respectively.

The change of the crystal structure of the powders changed their morphologies from needlelike shape to regular polyhedron shape, especially with 10 wt% NH_4Cl flux (Fig. 5). This excited result is different from the report [31], in which the morphologies of the powders from regular polyhedron shape to irregular shape with the increasing amount of NH_4Cl prepared by spray pyrolysis. The TG-DSC analysis of the Sr_2SiO_4 precursors without flux and with 5 wt% NH_4Cl is compared in Fig. 6. The small endothermic peak at 470 °C in Fig. 6(a) and (b) was due to precursor dehydration. Without adding any flux, the apparent weight loss in the system occurred at 913.5 °C, and no further weight loss occurred at temperatures higher than 950 °C (Fig. 6(a)). While adding 5 wt% NH_4Cl the corresponding temperatures advanced at 709.5 °C and lagged at 1150 °C (Fig. 6(b)), respectively. The reaction equation of $SrCO_3$ and SiO_2 system is given in Eq. (1).

$$2SrCO_3 + SiO_2 \rightarrow Sr_2SiO_4 + 2CO_2 \uparrow \quad (1)$$

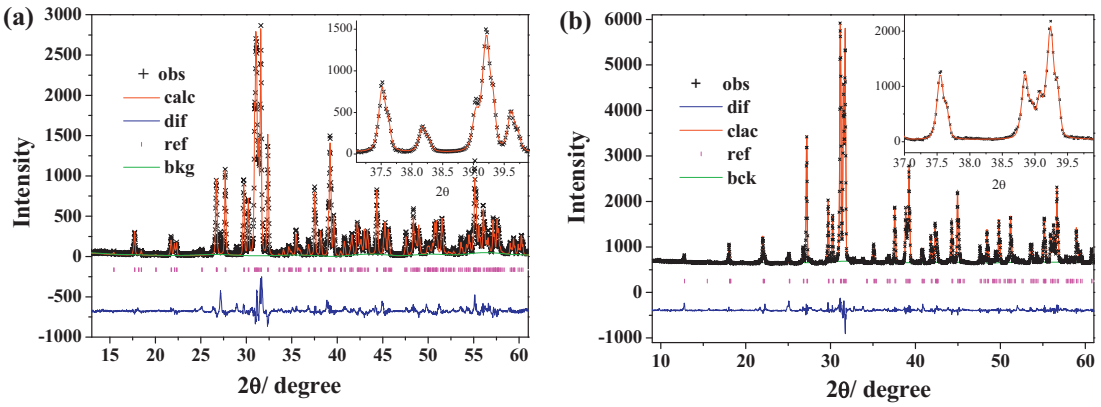

Fig. 4. Rietveld refinements (line) of the observed XRD patterns (+) for as-prepared β-Sr_2SiO_4 with 1 wt% NH_4Cl (a) and α′-Sr_2SiO_4 with 5 wt% NH_4Cl (b). Vertical bars below the patterns show the position of all possible reflection peaks of their phases. The lowest curve is the difference between the observed and the calculated intensities. The inset shows the characteristic peaks of them in 37–40°.

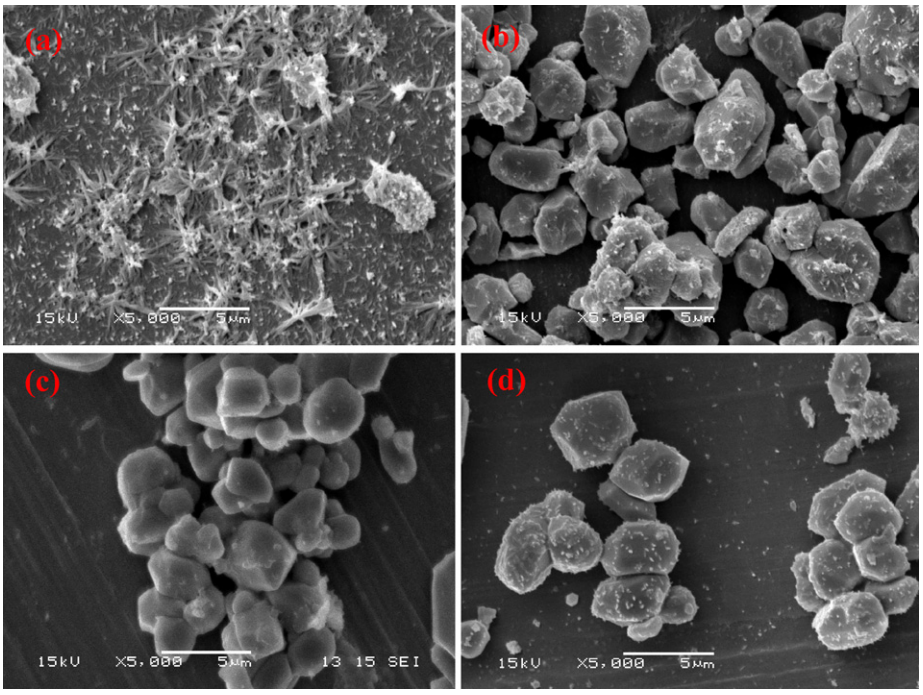

Fig. 5. SEM photographs of the $(Sr_{0.99}Dy_{0.01})_2SiO_4$ phosphors treated at 1000 °C for 4 h, with (a) 1 wt%, (b) 2 wt%, (c) 5 wt% and (d) 10 wt% NH_4Cl, respectively.

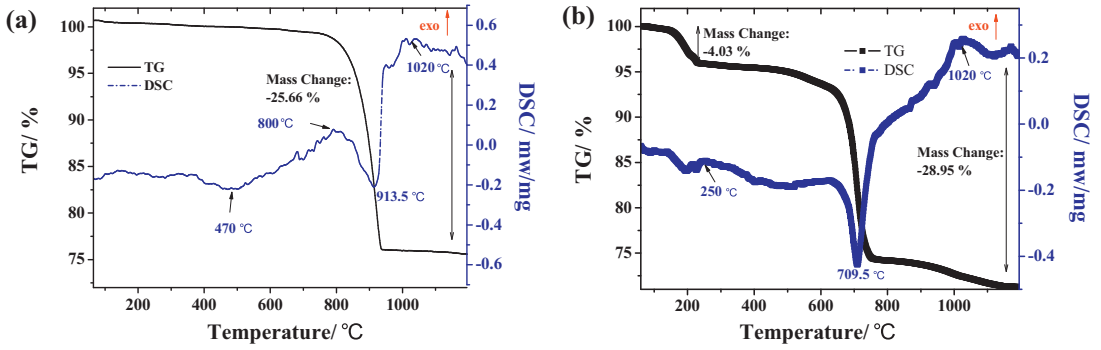

Fig. 6. TG–DSC analysis of the Sr_2SiO_4 precursor: (a) no flux and (b) adding 5 wt% NH_4Cl.

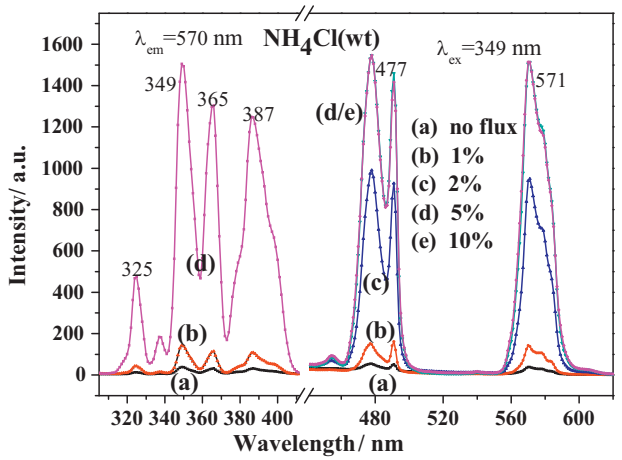

Fig. 7. Excitation spectra (left, λ_{em} = 570 nm) and emission spectra (right, λ_{ex} = 349 nm) of the $(Sr_{1.98}Dy_{0.01})_2SiO_4$ phosphors with different NH_4Cl adding amounts (wt%).

From TG curve of Fig. 6(a), the total weight loss amounted to 25.66%, which was closed to the theoretical weight loss of this reaction 24.41% according to calculation of Eq. (1). The difference was attributed to the dehydration. After adding 5 wt% NH_4Cl, the TG curve showed two stages including the 4.03% NH_4Cl volatilization around 250 °C and 28.95 – 4.03% = 24.92% CO_2 escape around 709.5 °C (their theoretical values were 5% and 23.25%). According to the Lu's report [32], no intermediate phase like SrO was detected in the range of 600–1000 °C and the Sr_2SiO_4 formation process was confirmed to be a direct reaction like Eq. (1). So the broad endothermic peak was attributed to the reaction of reactive strontium carbonate and silicon oxide. Based on the Hancock and Sharp's method [33,34], Lu's results [32] thought the reaction kinetics of Sr_2SiO_4 was guided by a single reaction mechanism and its formation mechanism was a three dimensional diffusion controlled process. In this solid state reaction, NH_4Cl as the flux plays a part in reaction process to accelerate the kinetics of the phase formation by enhancing diffusion coefficient. It helps us to synthesize powders with desirable properties, including fine size, narrow size distribution, high purity and good chemical homogeneity.

3.2. Luminescence properties of as-prepared phosphors

Fig. 7 (left) shows the excitation spectra of the prepared $Sr_2SiO_4:Dy^{3+}$ with different NH4Cl adding amounts. The sharp excitation peaks between 300 and 400 nm peaked at 325 nm, 349 nm, 365 nm, 387 nm and were due to the typical *f–f* transition of Dy^{3+}. The strongest line absorption was located at 349 nm, which was resulting from the $^6H_{15/2} \rightarrow {}^6P_{7/2}$ transition. Therefore, this phosphor could be applied to ultraviolet light emitting diodes. The excitation spectra of the αĭ-$Sr_2SiO_4:Dy^{3+}$ with 2–10 wt% NH_4Cl flux had higher peak intensities than those of the β-$Sr_2SiO_4:Dy^{3+}$ with 1 wt% NH_4Cl flux. The emission spectra (right) of all samples exhibited typically Dy^{3+} line emission at 477 nm (blue, $^4F_{9/2} \rightarrow {}^6H_{15/2}$) and 570 nm (yellow, $^4F_{9/2} \rightarrow {}^6H_{13/2}$, $\Delta L = 2$, $\Delta J = 2$). In Sun [29] and Lee's [25,31] reports for $Sr_2SiO_4:Eu^{2+}$, the β phase had a higher intensity than αĭ phase for any Eu^{2+} concentrations. But here, the α′-$Sr_2SiO_4:Dy^{3+}$ with 5 and 10 wt% NH_4Cl flux had the strongest luminescence. NH_4Cl flux improved the photoluminescence intensity of the $Sr_2SiO_4:Dy^{3+}$ phosphor by changing crystal structure (β → α′), particle size and surface property of the powders. The morphologies of α′-$Sr_2SiO_4:Dy^{3+}$ phosphor as show in Fig. 5(b)–(d) had large regular polyhedron shape and clean surface compared with needlelike shape of β phase, which could have higher photoluminescence intensity because of less surface defects. Fig. 8

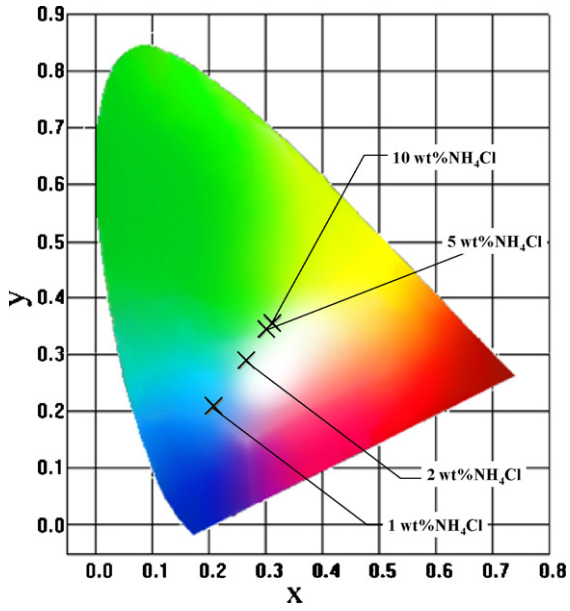

Fig. 8. CIE chromaticity coordinates of the $Sr_2SiO_4:Dy^{3+}$ phosphors with different addition amounts of NH_4Cl.

shows the CIE chromaticity coordinates of the $Sr_2SiO_4:Dy^{3+}$ phosphors. The colors of the $Sr_2SiO_4:Dy^{3+}$ phosphors changed from blue-green to white when the addition amount of NH_4Cl flux increased from 1 to 10 wt% of phosphors. For luminescent intensity, the $(Sr_{098}Dy_{0.02}Li_{0.02})_2SiO_4$ powders with the highest intensity in this study was selected to compare with the commercial phosphors, YAG:Ce^{3+} and $Sr_2SiO_4:Eu^{2+}$. The emission spectra of these three phosphors under their respective excitation wavelength are shown in Fig. 9. As can be seen from this figure, the intensity of $Sr_2SiO_4:Dy^{3+}$ reached almost 70.5% and 61.0% of YAG:Ce^{3+} and $Sr_2SiO_4:Eu^{2+}$, respectively. This originates from that the excitation spectrum of Dy^{3+} ions contains only narrow excitation band of *f–f* transition, which has no broad excitation such as *f–d* transition band or charge transfer band. This is a barrier for its application as SMWP. Even so, this can be overcome through charge compensation and sensitization to a certain extent. This enhanced luminescence of Dy^{3+} has been observed in $Ca_2B_2O_5$ [35], YVO_4 [36] by codoping Bi^{3+} and in $GdAl(BO_3)_4$ by codoping Ce^{3+}, and so on. Thus, for its applications in industry, further work is required to sensitize the luminescence of Dy^{3+} so as to highly enhance the luminescence intensity of this phosphor. Last but not least, the

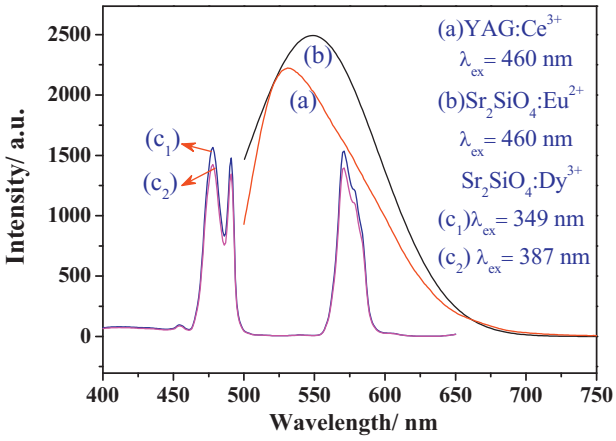

Fig. 9. Comparison of emission spectra of: (a) YAG:Ce^{3+}, λ_{ex} = 460 nm; (b) $Sr_2SiO_4:Eu^{2+}$, λ_{ex} = 460 nm; and $Sr_2SiO_4:Dy^{3+}$ (c_1) λ_{ex} = 349 nm, (c_2) λ_{ex} = 387 nm.

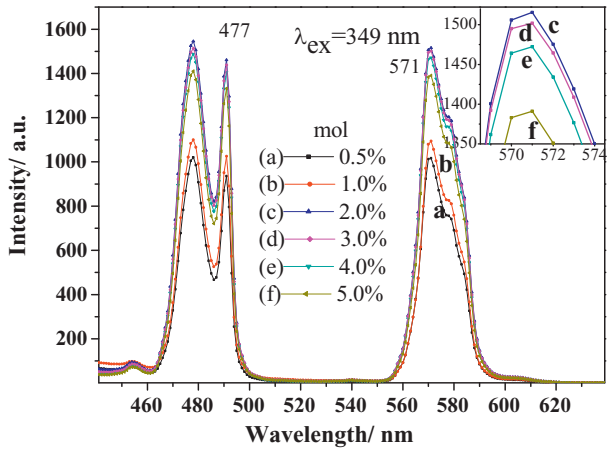

Fig. 10. Emission spectra of $(Sr_{1-x}Dy_x)_2SiO_4$ phosphors under UV excitation (λ_{ex} = 349 nm).

emission spectrum of Sr_2SiO_4:Dy^{3+} excited by 387 nm was similar with that excited by 349 nm except for its slightly weaker intensity in Fig. 9, and the FWHM of excitation peak of 387 nm was larger than that of 349 nm in Fig. 7. These indicate that Sr_2SiO_4:Dy^{3+} powders have great potential as candidates for white LEDs pumped by a UV chip (380–400 nm). However, in order to investigate the mechanism of energy transfer and concentration quenching, 349 nm as the strongest excitation peak was still adopted as the excitation wavelength.

Fig. 10 shows the emission spectra of $(Sr_{1-x}Dy_x)_2SiO_4$ phosphors prepared with 5 wt% NH_4Cl under 1000 °C for 4 h (λ_{ex} = 349 nm). The inset in Fig. 10 displays the magnification for the intensity of 571 nm. With increasing Dy^{3+} concentration the relative intensity of 571 nm increased and no blue or red shift was observed. The optimum doping concentration of Dy^{3+} was found to be 2.0 mol% and then a concentration quenching appeared.

As we know, the self-concentration quenching is mostly due to the interaction of the electric multipoles during the resonance transfer. According to the L. Ozawa's report [37], the concentration beginning to quench should be equal to $1/(1+Z)$ in this case. Z is the number of the nearest neighbor cations around lighting center ions. And the relationship between the luminescent intensity (I) and the concentration of activators (x) should be expressed by $I = Bx(1-x)^Z$ (B is a constant). Then Z is obtained by the operation of logarithmic transformation. Fig. 11(a) is The relational curve of $\lg(I/x_{Dy}) \sim \lg(1-x_{Dy})$ for the emission (571 nm). After linear fitting for all data points, the slope of this straight line Z was 43.098. And $1/(1+Z) \approx 0.023$. It is very close to the critical concentration of self-quenching (2.0 mol%). So it is reasonable to use the interaction of the electric multipoles to understand its self-concentration quenching of $^4F_{9/2} \rightarrow {}^6H_{13/2}$ transition. In Dexter's theory [38] for the determination of interaction type of the electric multipoles, the relationship between the luminescent intensity (I) and the concentration of activators (x) should be expressed by $\lg(I/x) = A - (\theta/3)\lg(x)$. Here, A is a constant for one host. When the value of θ is 6, 8 and 10, the interaction type is dipoles–dipoles (d–d), dipoles–quadrupoles (d–q) and quadrupole–quadrupoles (q–q), respectively. The relational curve $\lg(I/x_{Dy})$ and $\lg(x_{Dy})$ is plotted in Fig. 11(b).

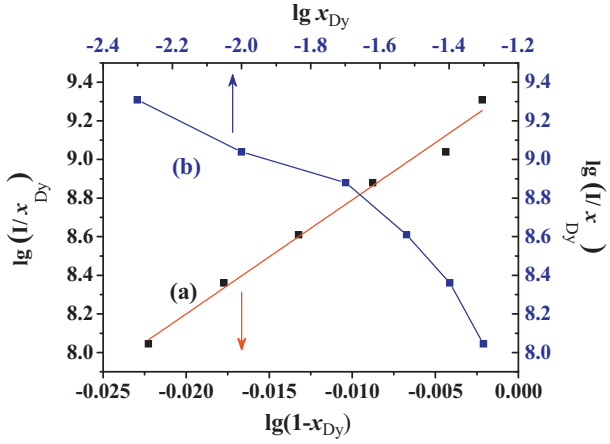

Fig. 11. The relational curves of $\lg(I/x_{Dy}) \sim \lg(1-x_{Dy})$ (a) and $\lg(I/x_{Dy}) \sim \lg(x_{Dy})$ (b) for the emission(571 nm) (λ_{ex} = 349 nm).

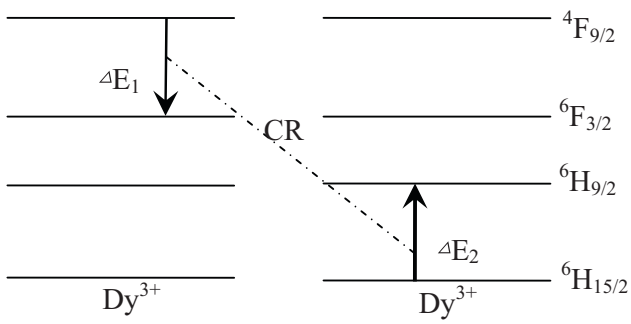

Fig. 12. The schematic plan for cross-relaxation of Dy^{3+} ions.

According to the slope of the straight part of curve (b) caused by the concentration quenching, θ is approximately equal to 6.09. As stated in Dexter's theory [38], this indicates that the mechanism of self-concentration quenching of $^4F_{9/2} \rightarrow {}^6H_{13/2}$(571 nm) transition is derived from the interaction between electric dipoles and electric dipoles (d–d). In the same method, the self-concentration quenching of $^4F_{9/2} \rightarrow {}^6H_{15/2}$(477 nm) transition is also caused by the d–d interaction. Meanwhile, this behavior may caused by the cross relaxation. In fact, there is a good match between the $^4F_{9/2} \rightarrow {}^6F_{3/2}$ transition energy (about 7800 cm^{-1}) and $^6H_{15/2} \rightarrow {}^6H_{9/2}$ (about 7400 cm^{-1}) (Fig. 12). Such a small energy difference can be easily bridged with the help of few phonons. As we know, the probability of cross relaxation and the energy transfer rate are proportional to R^{-3} under the d–d interaction (R is the distance of the nearest neighbor Dy^{3+} ions) [39]. With a low concentration doping, R is too large to occur the cross relaxation. And the energy is mostly consumed by light emitting. But under a higher concentration, R decreases dramatically and the cross relaxation enhance obviously. The nonradiative energy transition is also enhanced by the increasing transfer probability of $^4F_{9/2} \rightarrow {}^6F_{3/2}$. So the luminescence is quenched and the intensity decrease.

Furthermore, from Figs. 7 and 10, the intensity of blue light ($^4F_{9/2} \rightarrow {}^6H_{15/2}$) was slightly higher than yellow light ($^4F_{9/2} \rightarrow {}^6H_{13/2}$, $\Delta L = 2$, $\Delta J = 2$). In the previous reports, only in borate glass [40], the intensities of two emission bands of Dy^{3+} ions are equal. In the most hosts, the intensity of yellow light is higher than that of blue light [35,41,42]. The yellow band corresponds to the hypersensitive transition and is easily affected by the environment, especially by the site symmetry of Dy^{3+}. When Dy^{3+} is located at a site of high symmetry with an inverse center, it displays no luminescence [43]. And it is a forced electric dipole transition being allowed only at low symmetries with no inversion center. Meanwhile, at a site deviated from an inverse center, the yellow emission is prominent in the emission spectrum [44,45]. Since the emission intensity of $^4F_{9/2} \rightarrow {}^6H_{15/2}$ is slightly higher than that of the $^4F_{9/2} \rightarrow {}^6H_{13/2}$, which indicates that Dy^{3+} ions substitute Sr^{2+} ions with low symmetry. The α′-Sr_2SiO_4 host belongs to the low-symmetry orthorhombic system (space group: *Pnma*, and the

Table 1
Variation in yellow-to-blue intensity ratio (*Y/B*) with concentration of Dy^{3+} in Sr_2SiO_4:Dy^{3+}.

x (Dy^{3+}, mol%)	0.5	1.0	2.0	3.0	4.0	5.0
Y/B	0.91	0.87	0.90	0.92	0.91	0.91

radius of Dy^{3+} ion (0.91 Å) is much smaller than that of Sr^{2+}ion (1.12 Å)), so some Dy^{3+} ions may enter into the host interstices and act as emission center. The variation in yellow-to-blue intensity ratio (*Y/B*) with concentration of Dy^{3+} in Sr_2SiO_4:Dy^{3+} is shown in Table 1. The *Y/B* value resembled not to change with varying the Dy^{3+} concentration. This point is not coincident with the theory supported by Su [43]. This non-equivalent substitution of Dy^{3+} to Sr^{2+} would form more defects and the surrounding and local symmetry would change with increasing concentration of Dy^{3+}. In our experiment, Li^+ ions as charge compensation ions would weaken this effect, that is, Li^+ ions is also a indispensable element for steadying the emission color of Dy^{3+} in the related non-equivalent substitution.

4. Conclusions

We successfully synthesized single and pure β- and α′-Sr_2SiO_4:Dy^{3+} phosphors with desired morphology using the solid-state reaction method only by changing the amount of NH_4Cl flux. The key synthesized conditions for pure β- and α′-Sr_2SiO_4 were the mounts of NH_4Cl of 1.0 wt% and 2.0–5.0 wt%, respectively, and then the matching calcination system of 1000 °C for 4 h. NH_4Cl played a part in reaction process to accelerate the kinetics of the phase formation by enhancing diffusion coefficient to help us to synthesize powders with desirable properties including high purity, fine size and further enhanced luminescence. The as-prepared phosphors showed characteristic blue and yellow emission of Dy^{3+} ions, and the intensity of Dy^{3+} in αĭ-phase was higher than that of Dy^{3+} in β-phase. The optimum concentration of Dy^{3+} was 2.0 mol% and then the concentration quenching were caused by the d–d interaction and a cross relaxation effect. In all emission spectrum, the intensity of $^4F_{9/2} \rightarrow {}^6H_{15/2}$ transition was slightly higher than that of $^4F_{9/2} \rightarrow {}^6H_{13/2}$ ($\Delta L = 2$, $\Delta J = 2$) transition owing to the low-symmetry around Dy^{3+} ions. In our investigations, the colors of the Sr_2SiO_4:Dy^{3+} phosphors changed from blue-green to white with increasing amounts of NH_4Cl. And the *Y/B* value did not change with varying the Dy^{3+} concentration using Li^+ ions for charge compensation. This phosphor exhibited brighter white light emitting and its luminescence intensity reached almost 70.5% and 61.0% of YAG:Ce^{3+} and Sr_2SiO_4:Eu^{2+}, respectively, These indicate that this phosphor has a good possibility as phosphor candidates used for white LEDs pumped by a UV chip and the promising enhancement of light-emitting efficiency will promote its unbounded applications in industry.

Acknowledgements

The authors gratefully acknowledge the financial support for this work from the Natural Science Foundation of Jiang Su Province (BK2007724) and National Defense Fundamental Research of China (6134502-1).

References

[1] R.V. Steele, Nature Photonics 1 (2007) 25–26.
[2] D.A. Steigerwald, J.C. Bhat, D. Collins, R.M. Fletcher, M.O. Holcomb, M.J. Ludowise, P.S. Martin, S.L. Rudaz, IEEE J. Sel. Top. Quant. 8 (2002) 310–320.
[3] M.A. Greenwood, Photon. Spectra 42 (2008), p. 100–100.
[4] Y. Narukawa, I. Niki, K. Izuno, M. Yamada, Y. Murazaki, T. Mukai, Jpn. J. Appl. Phys. Part 2 41 (2002) L371–L373.
[5] D.J. Robbins, J. Electrochem. Soc. 126 (1979) 1550–1555.
[6] S. Johnson, J. Simmons, Materials for solid state lighting, in: Materials Research Society Spring Meeting 2002, San Francisco, 2002.
[7] M.R. Krames, O.B. Shchekin, R. Mueller-Mach, G.O. Mueller, L. Zhou, G. Harbers, M.G. Craford, J. Disp. Technol. 3 (2007) 160–175.
[8] N. Narendran, Y. Gu, J.P. Freyssinier, H. Yu, L. Deng, J. Cryst. Growth 268 (2004) 449–456.
[9] Y. Narukawa, J. Narita, T. Sakamoto, T. Yamada, H. Narimatsu, M. Sano, T. Mukai, Phys. Status Solidi A 204 (2007) 2087–2093.
[10] J.S. Kim, K.T. Lim, Y.S. Jeong, P.E. Jeon, J.C. Choi, H.L. Park, Solid State Commun. 135 (2005) 21–24.
[11] J.S. Kim, P.E. Jeon, Y.H. Park, J.C. Choi, H.L. Park, G.C. Kim, T.W. Kim, Appl. Phys. Lett. 85 (2009) 3696–3698.
[12] J.S. Kim, A.K. Kwon, Y.H. Park, J.C. Choi, H.L. Park, G.C. Kim, J. Lumin. 122–123 (2007) 583–586.
[13] J. Zhou, Y. Wang, B. Liu, F. Li, J. Appl. Phys. 108 (2010), 033106-033106-5.
[14] C.K. Chang, T.M. Chen, Appl. Phys. Lett. 91 (2007), 081902-081902-3.
[15] W.-S. Song, Y.-S. Kim, H. Yang, Mater. Chem. Phys. 117 (2009) 500–503.
[16] J.S. Kim, P.E. Jeon, J.C. Choi, H.L. Park, Solid State Commun. 133 (2005) 187–190.
[17] N. Lakshminarasimhan, U.V. Varadaraju, J. Electrochem. Soc. 152 (2005) H152–H156.
[18] W.H. Hsu, M.H. Sheng, M.S. Tsai, J. Alloys Compd. 467 (2009) 491–495.
[19] L. Zhang, Z.L. Zhao, E.T. Xu, L.L. Feng, X.X. Wu, Q.T. Zhang, J. Funct. Mater. 40 (2009), 1249–1250+1254.
[20] A.C. Larson, R.B. Von Dreele, Los Alamos National Laboratory Report LAUR 8 (1994) 6–748.
[21] B.H. Toby, J. Appl. Cryst. 34 (2001) 210–213.
[22] X. Li, Z.P. Yang, L. Guan, C. Liu, P.L. Li, J. Cryst. Growth 310 (2008) 3117–3120.
[23] H.Y. Koo, S.K. Hong, Y.C. Kang, J. Ceram. Process Res. 8 (2007) 243–247.
[24] H.S. Kang, Y.C. Kang, K.Y. Jung, S.B. Park, Mater. Sci. Eng. B-Solid State Mater. Adv. Technol. 121 (2005) 81–85.
[25] J.H. Lee, Y.J. Kim, Mater. Sci. Eng. B 146 (2008) 99–102.
[26] H. He, R.L. Fu, X.F. Song, D.L. Wang, J. Chen, J. Lumin. 128 (2008) 489–493.
[27] N. Lakshminarasimhan, U.V. Varadaraju, Mater. Res. Bull. 43 (2008) 2946–2953.
[28] S.H.M. Poort, H.M. Reijnhoudt, H.O.T. van der Kuip, G. Blasse, J. Alloys Compd. 241 (1996) 75–81.
[29] X. Sun, J. Zhang, X. Zhang, Y. Luo, X. Wang, J. Rare Earth 26 (2008) 421–424.
[30] Z. Pan, H. He, R. Fu, S. Agathopoulos, X. Song, J. Lumin. 129 (2009) 1105–1108.
[31] S.H. Lee, H. Young, Koo, Y.C. Kang, Ceram. Int. 36 (2010) 1233–1238.
[32] C.-H. Lu, P.-C. Wu, J. Alloys Compd. 466 (2008) 457–462.
[33] J. Hancock, J. Sharp, J. Am. Ceram. Soc. 55 (1972) 74–77.
[34] W.A. Johnson, K.F. Mehl, Trans. Am. Inst. Mining Met. Eng. 135 (1939) 416–458.
[35] Q. Su, Z. Pei, J. Lin, F. Xue, J. Alloys Compd. 225 (1995) 103–106.
[36] Z.P. Ci, Y.H. Wang, J.C. Zhang, Chin Phys. B 19 (2010), 057803-057803-6.
[37] L. Ozawa, J. Electrochem. Soc. 126 (1979) 106–109.
[38] D.L. Dexter, J.H. Schulman, J. Chem. Phys. 22 (1954) 1063–1071.
[39] X. Xu, M. Su, Luminescence Theory and Luminescent Materials, Chemical Industry Press, Beijing, 2004.
[40] G.S. Raghuvanshi, H.D. Bist, H.C. Kandpal, J. Phys. Chem. Solids 43 (1982) 781–783.
[41] Z. Pei, Q. Su, S. Li, J. Lumin. 50 (1991) 123–126.
[42] Q. Su, H. Liang, C. Li, H. He, Y. Lu, J. Li, Y. Tao, J. Lumin. 122–123 (2007) 927–930.
[43] Q. Su, Z. Pei, L. Chi, H. Zhang, Z. Zhang, F. Zou, J. Alloys Compd. 192 (1993) 25–27.
[44] E. Cavalli, M. Bettinelli, A. Belletti, A. Speghini, J. Alloys Compd. 341 (2002) 107–110.
[45] Z. Xiu, S. Liu, M. Ren, J. Liu, J. Pan, X. Cui, J. Alloys Compd. 425 (2006) 261–263.